Journal of the Serbian Chemical Society
JSCS-info@shd.org.rs • www.shd.org.rs/JSCS

ACCEPTED MANUSCRIPT

Journal of the Serbian Chemical Society
JSCS-info@shd.org.rs • www.shd.org.rs/JSCS
J. Serb. Chem. Soc. **00(0)** 1-12 (2025)
JSCS–13327
Original scientific paper
Published DD MM, 2025

Removal of nickel(II) ions during water purification with ferrous sulfate. Part 2. Structure and composition of iron(III) hydroxide precipitates

OLEG D. LINNIKOV*, IRINA V. RODINA, GALINA S. ZAKHAROVA, INNA V. BAKLANOVA, YULIA V. KUZNETSOVA, ALEXANDER P. TYUTYUNNIK, ZILARA A. FATTAKHOVA

Institute of Solid State Chemistry, Ural Branch of the Russian Academy of Sciences, Pervomayskaya St., 91, 620990, Ekaterinburg, Russia.

(Received 7 April; revised 28 April; accepted 30 October 2025)

Abstract: A comparative analysis of the composition and structure of freshly precipitated iron(III) hydroxide precipitates obtained from a solution of iron(II) sulfate in the presence of sodium sulfate (400 mg L^{-1}) at pH 7 and 8 before and after sorption of nickel ions on them was carried out. Using IR and Raman spectroscopy, X-ray phase and thermogravimetric analysis, it was shown that the precipitates have the general (gross) formula $Fe_2O_3 \times 2H_2O$ and contain a small amount of goethite (α-FeOOH) and lepidocrocite (γ-FeOOH). It has been established that the sorption of nickel ions on these precipitates is not accompanied by chemisorption, i.e. no mixed compounds between iron and nickel are formed. The point of zero charge of precipitation particles is at pH 5.4, with positive zeta potential below and negative above this pH. The introduction of nickel ions into the solution leads to the appearance of a second zero charge point at pH 10.2.

Keywords: iron(III) hydroxide; iron(II) sulfate; nickel ions; IR and RAMAN spectroscopy; X-ray and thermogravimetric methods of analysis; zeta potential.

INTRODUCTION

In the first part of this work, it was shown that iron(III) hydroxide, formed during the hydrolysis of $FeSO_4$ coagulant in the presence of sodium sulfate (400 mg L^{-1}) at pH 7 and 8, has a high sorption capacity with respect to divalent nickel ions.[1] However, the structure and composition of the resulting precipitate were not studied in detail. Therefore, it remained unclear which iron(III) compound was the sorbent in this case. The fact is that the precipitation of iron(III) hydroxide from solutions of divalent iron salts occurs due to the oxidation of the latter by atmospheric oxygen present in dissolved form in the solution and at low

* Corresponding author. E-mail: linnikov@mail.ru
https://doi.org/10.2298/JSC250407081L

concentrations of iron(II) ions can be described by a generalizing reaction equation:

$$4Fe^{2+} + O_2 + 2H_2O + 8OH^- \rightarrow 4Fe(OH)_3\downarrow$$

However, according to literature data, the precipitate of iron(III) hydroxide formed in this case does not always correspond to the general (gross) formula $Fe(OH)_3$.[2-6] For example, previous studies of iron(III) hydroxide precipitates formed by hydrolysis of the coagulant $FeCl_3$ in the presence of sodium sulfate (400 mg L^{-1}) at pH 7 and 8 showed the formation of two-line ferrihydrite with the general (gross) formula $Fe_2O_3 \times 3H_2O$.[7] At the same time, these precipitates also have a high sorption capacity with respect to nickel ions.[7]

The purpose of this part of the work is to study the physicochemical properties, composition and structure of iron(III) hydroxide precipitate formed during the hydrolysis of $FeSO_4$ coagulant.

EXPERIMENTAL

Iron(III) hydroxide precipitates with adsorbed nickel ions were obtained in coagulation experiments according to the technique described earlier.[1] The studies were carried out in laboratory conditions at room temperature (25±2°C) using a model solution containing 400 mg L^{-1} sodium sulfate. Nickel ions were introduced into the solution in the form of a $NiSO_4$ solution with a concentration of 10 mg L^{-1}. Iron(III) hydroxide precipitates were obtained at pH 7 and 8 by adding 10 g L^{-1} NaOH solution to the model solution. The mixture was continuously stirred on a magnetic stirrer to maintain the resulting iron(III) hydroxide precipitate in suspension. After 30 minutes, the stirrer was turned off and the formed precipitate of iron(III) hydroxide was separated from the solution by filtration through blue ribbon filter paper (Russia). The next step was the washing of iron(III) hydroxide precipitate several times on the filter with distilled water followed by drying at room temperature.

Iron(III) hydroxide precipitates without nickel ions adsorbed on them were obtained in a similar manner without introducing nickel ions into the model solution.

Analysis and characterization

The morphology of precipitates was studied using a scanning electron microscope (SEM) JSM-6309LA from JEOL (Japan).

The zeta potential of iron(III) hydroxide precipitate particles was determined using electrophoretic light scattering with a Zetasizer Nano ZS device (Malvern Panalytical Ltd.) during the precipitation reaction by taking aliquots at different pH. To prepare the test solution, the required amount of $FeSO_4$ solution (13.57 g L^{-1}) was introduced into a given volume of the model solution with continuous stirring on a magnetic stirrer. After that, the solution was slowly alkalized with NaOH solution (10 g L^{-1}). After each alkalinization and establishment of equilibrium in the solution, the aliquot was taken and used for the zeta potential measurements. The initial concentration of iron(II) ions in the solution was 12.5 mg L^{-1}.

Another similar experiment was carried out in the presence of nickel ions in the solution, which were introduced into the model solution before adding the $FeSO_4$ solution. The concentration of nickel ions in the solution before alkalization was 10 mg L^{-1}.

The IR absorption spectrum of iron (III) hydroxide precipitates in the wave number range of 4000–400 cm^{-1} was recorded using a Vertex 80 infrared-Fourier spectrometer by Brooker,

using an attenuated total internal reflection (ATR) MVP-Pro attachment (Harrick, prism material diamond).

Raman spectra were recorded in the wave number range of 4000-50 cm^{-1} at room temperature using an InVia Reflex RENISHAW dispersive Raman spectrometer (λ=532 nm wavelength, P=1-5 mW laser power).

Thermogravimetric analysis of iron(III) hydroxide precipitates was performed using a STA 449 F3 Jupiter thermal analyzer (Netzsch), combined with a QMS 403 quadrupole mass spectrometer, in an air atmosphere, at a heating rate of 10 °C min^{-1}.

X-ray phase analysis of precipitates was carried out using a STOE STADI-P X-ray powder diffractometer.

RESULTS AND DISCUSSION

SEM images of the iron(III) hydroxide precipitates formed in the model solution are shown in Fig. 1. All iron(III) hydroxide precipitates obtained in this study consisted of very small particles that aggregated into larger structures. Externally, they appear as loose, dark-brown formations. After filtration, washing with distilled water, and air drying at room temperature, the precipitates compacted, became more solid, and reduced in volume significantly.

The diffraction patterns of iron(III) hydroxide precipitates are shown in Fig. 2 and indicate the similar structure of precipitates. The blurred appearance of the peaks in the diffraction patterns indicates the nanometer size of the precipitate particles and their weak crystallinity.

XRD patterns analysis showed that when iron(III) hydroxide is precipitated at pH 7 and 8 without nickel ions in the model solution, the resulting precipitates consist of a mixture of two phases: goethite (α-FeOOH) and lepidocrocite (γ-FeOOH) (Fig. 2, curves 1 and 2). The ratio of these phases depends on the pH of the solution. Thus, at pH 7, goethite comprises approximately 62 wt% of the precipitate, while lepidocrocite accounts for 38 wt%. At pH 8, the proportion of goethite increases to 81 wt%, with lepidocrocite decreasing to 19 wt%. In the presence of nickel ions during precipitation, the phase composition of the resulting precipitates changes insignificantly (Fig. 2, curves 3 and 4). At pH 7, the precipitate still contains approximately 62 wt% goethite and 38 wt% lepidocrocite. However, at pH 8, lepidocrocite is replaced by magnetite (Fe_3O_4), which appears in an amount of about 38 wt%, while the goethite content remains unchanged at approximately 62 wt%. This formation of magnetite may be facilitated by the higher pH of the solution. None of the diffraction patterns indicated the presence of a new phase containing nickel ions. Subsequent thermal analysis (see below) resulted in the decomposition of the precipitates, and the samples consisted of hematite and magnetite. An example of such a diffraction pattern is shown in Fig. 2 (curve 5).

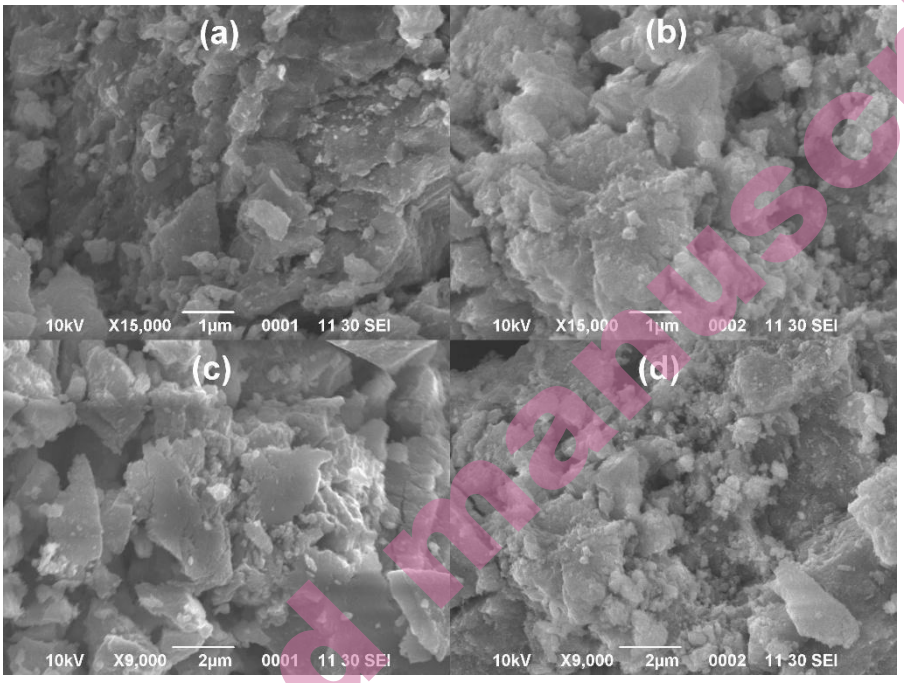

Fig. 1. SEM image of iron(III) hydroxide precipitate obtained from the model solution: a and b - precipitation at pH 7 and 8, respectively; c and d - precipitation in the presence of nickel ions in solution at pH 7 and 8, respectively.

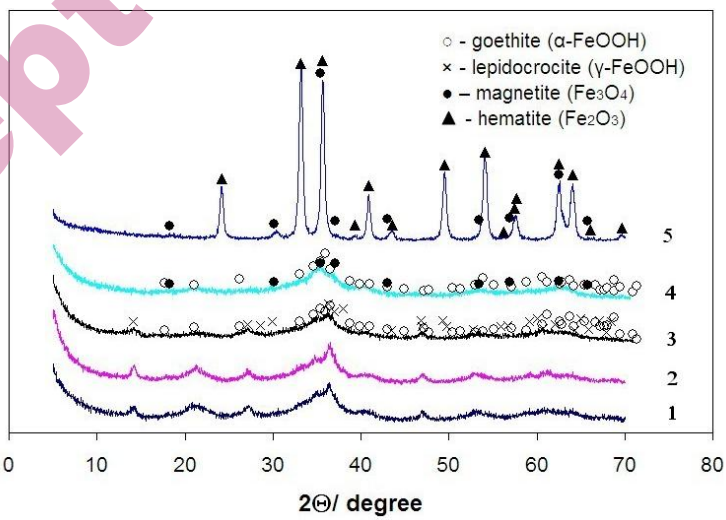

Fig. 2. X-ray powder diffraction patterns of iron(III) hydroxide precipitates after drying in air at room temperature (25±2 °C): 1 and 2 - precipitation at pH 7 and 8, respectively; 3 and 4 - precipitation in the presence of nickel ions in solution at pH 7 and 8, respectively; 5 – precipitate after thermal analysis obtained at pH 7 in the presence of nickel ions in solution.

Raman spectra of iron(III) hydroxide precipitates obtained at pH 7 and 8 and different power of the irradiating laser are shown in Fig. 3. It can be seen from Fig. 3 that with increasing laser power (P), a change in the shape of the obtained Raman spectrum is observed. If at P=1 mW the spectrum is a curve on which not a single line is fixed (Fig. 3, curves 1), then at a laser power of 5 mW (Fig. 3, curves 2) the shape of the spectrum changes, and lines corresponding to hematite (α-Fe_2O_3) appear in it: 211-215 (A_{1g}), 272-283, 379-389, 457-476, 568-588 and 616-689 cm^{-1} (E_g), ~1300 cm^{-1} (second harmonic). This indicates the destruction of precipitate at a given power of the irradiating laser. The observed rise in the background is most likely associated with fluctuations in CO_3^{2-} and their overtones. It should be noted that thermogravimetric analysis (see below) also showed the presence of small amounts of carbonates in the precipitates. The observed decomposition of iron(III) hydroxide precipitate with an increase in the power of the irradiating laser is in good agreement with the data,[7,8] where a similar destruction of ferrihydrite was recorded during the recording Raman spectra, as well as the transformation of magnetite into maghemite and hematite.[9]

Thus, recording the Raman spectrum at low laser power (1 mW) did not record lines characteristic of OH groups, which should be part of the precipitate if it corresponds to the general (gross) formula FeOOH (or $Fe(OH)_3$). In addition, the spectrum does not contain lines characteristic of goethite (α-FeOOH) and lepidocrocite (γ-FeOOH),[8-10] which indicates the absence of these phases in the precipitate. This result does not agree with the X-ray phase analysis data (see above).

The IR spectra of the obtained iron(III) hydroxide precipitates are shown in Fig. 4, from which it can be seen that they are close to each other. On all IR spectra of iron(III) hydroxide precipitates, an intense wide band is present in the frequency range of stretching vibrations of water molecules $\nu(H_2O)$ at 3139-3209 cm^{-1}. At 1628-1635 cm^{-1}, the bending mode of water molecules $\delta(H_2O)$ is recorded. The bands at 1100-1122 cm^{-1} can be attributed to the stretching asymmetric vibrations of $\nu_3(SO_4^{2-})$. The presence of these bands indicates the presence of traces of unwashed sodium sulfate in the precipitates. The asymmetric and symmetric stretching vibrations $\nu(CO_3^{2-})$ appear as broad bands at 1493-1500, 1333-1359 and 1018-1093 cm^{-1}, and the deformation vibrations $\delta(CO_3^{2-})$ appear at 883-887 cm^{-1}. These bands are probably caused by the presence of carbonates in the formed precipitates, the presence of which was mentioned above. The stretching asymmetric and symmetric vibrations of the C-H bond are manifested at 2887-2890 cm^{-1} and 2817-2925 cm^{-1}, respectively. The appearance of these bands in the IR spectra of the precipitates can be attributed, as the analysis indicates, to the presence of small organic impurities in the initial NaOH reagent used to prepare a solution of sodium hydroxide (10 g L^{-1}) for alkalizing the model solution during experiments. In addition, a small impurity of iron(III) hydroxocarbonate

($FeOHCO_3$) may also be present in the precipitate. This compound could have formed during the precipitation of iron(III) hydroxide with NaOH solution, as the latter typically contains sodium carbonate (Na_2CO_3) as an impurity. Moreover, the absorption of carbon dioxide from the air by the solution during the experiment may have contributed to its formation.

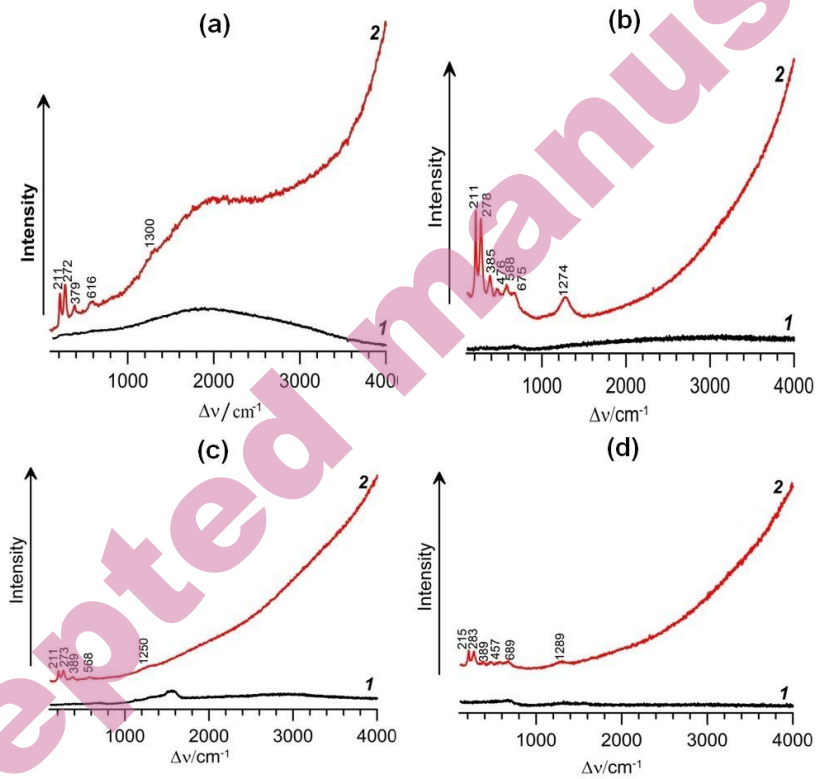

Fig. 3. Raman spectra of iron(III) hydroxide precipitate obtained at pH 7 and 8: a and c - precipitation at pH 7 and 8, respectively; b and d - precipitation in the presence of nickel ions in solution at pH 7 and 8, respectively; 1 – survey at P=1 mW; 2 – survey at P=5mW (survey duration in all cases is 10 seconds).

For all samples, the bands from bending vibrations of C-H bonds are superimposed on modes with frequencies 883-885 cm^{-1} belonging to the CO_3^{2-}-ion. Bands 786-787 and 618-651 cm^{-1} can be attributed to bending vibrations of C-H and C-C bonds. Frequencies below 600 cm^{-1} can be attributed to Fe-O vibrations. The region below 1100 cm^{-1} contains mainly bands belonging to CO^{2-}- ions and organic impurities. The observed differences in the IR spectra of the samples in the region below 1100 cm^{-1} are apparently explained by the different adsorption values of these impurities on the formed iron(III) hydroxide precipitate. None of

the IR spectra, as well as earlier Raman spectra, showed intense absorption bands characteristic of OH groups that are not part of water and belong to the iron(III) hydroxide precipitate, if it corresponded to the general (gross) formula FeOOH or $Fe(OH)_3$.

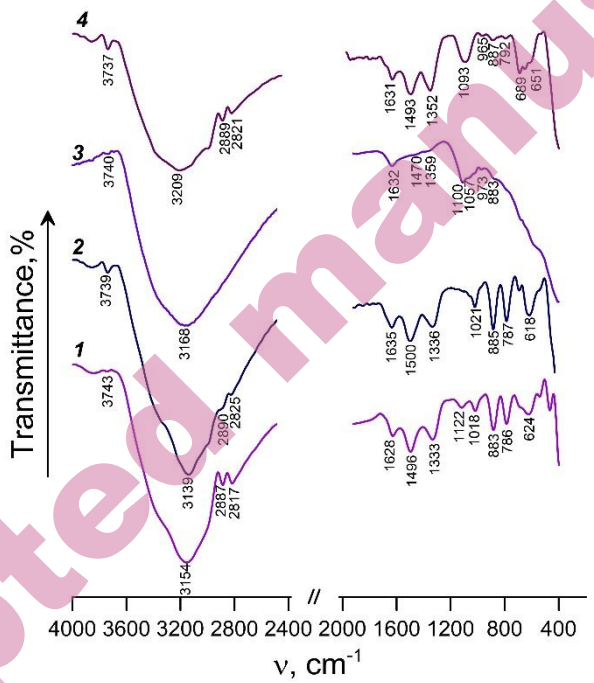

Fig. 4. IR spectra of iron(III) hydroxide precipitates: 1 and 2 – precipitation at pH 7 и 8, respectively; 3 and 4 – precipitation in the present of nickel ions (10 mg L^{-1}) in solution at pH 7 and 8, respectively.

Fig. 5 shows the results of thermogravimetric analysis of the formed iron(III) hydroxide precipitated at pH 7 and 8 in the absence (Figs. 5a and 5c) and presence (Figs. 5b and 5d) of nickel ions (10 mg L^{-1}). As can be seen, thermograms of all precipitates demonstrate similar trends. Already with slight heating, water (MS curves m/z=18 a.u.m.) and carbon dioxide (MS curves m/z=44 a.u.m.) begin to be removed from precipitates. Moreover, much more carbon dioxide is released from the precipitates obtained in the presence of nickel ions in solution (Figs. 5b and 5d). This may be due to the higher content of organic impurities in these samples.

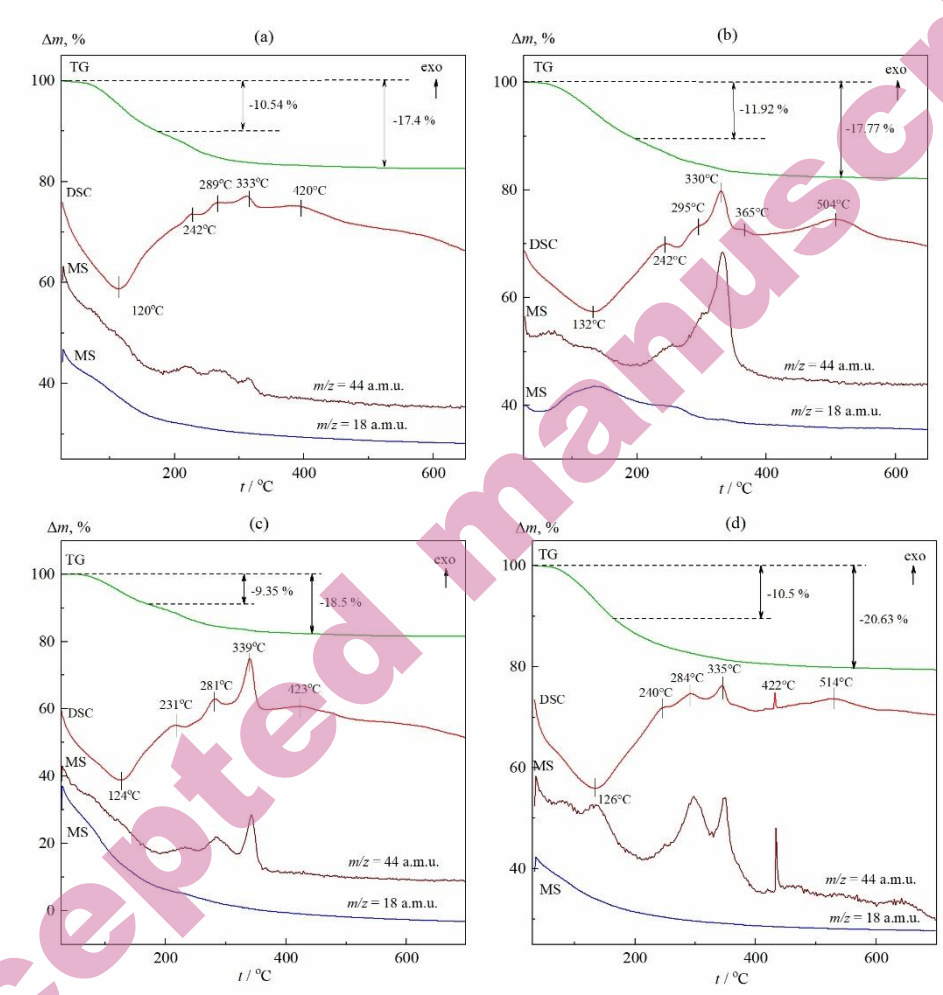

Fig. 5. Thermogravimetric (TG, green), DSC (red), and mass spectroscopy (MS, brown, blue) curves of iron(III) hydroxide precipitated from the model solution at pH 7 (a and b) and 8 (c and d): (a), (c) - there are no nickel ions in the solution; (b), (d) - precipitation in the presence of nickel ions (10 mg L^{-1}) in the solution. Δm is the change in the mass of the precipitate; t is the temperature, °C.

The mass loss of the precipitates occurs in a stepwise manner. Approximately 9-12% of the mass is lost at the first stage, followed by an additional loss of about 9% in the second stage, resulting in a total mass decrease of around 18%. It should be noted that several peaks in carbon dioxide release are observed, indicating the sequential decomposition of carbon-containing compounds into CO_2. The process is accompanied for all samples by weak exoeffects at temperatures 231-242, 281-295, 330-339. The exoeffects observed at 365-423, 504 and 514°C likely

correspond to the crystallization process of hematite (α-Fe_2O_3) and magnetite (Fe_3O_4), as confirmed by X-ray phase analysis. So, after thermogravimetric analysis, the precipitate corresponding to Fig. 5a consisted of hematite, and the precipitate corresponding to Fig. 5b contained approximately 86.3 wt% hematite and 13.7 wt% magnetite (Fig. 2, curve 5). The formation and stability of the magnetite during thermal analysis is probably attributed to the presence of carbonates and organic compounds in the precipitates. The observed release of carbon dioxide is probably due to both its desorption from the samples and the gradual thermal decomposition of organic and carbonate impurities, the presence of which is recorded by IR spectra (Fig. 4). Analysis revealed a total carbon content in the samples ranging from 0.73 to 1.2 wt%. Therefore, the mass loss during heating was mainly due to dehydration. Considering that Raman and IR spectra did not confirm the presence of non-aqueous OH groups in the samples, and also taking into account the observed mass loss of about 18%, we assign them the general (gross) formula $Fe_2O_3 \times 2H_2O$. It should be noted that if the precipitates consisted of goethite and lepidocrocite, then, given the absence of non-aqueous OH groups in their structure, they would have a general (gross) formula $Fe_2O_3 \times H_2O$, and the loss of precipitate mass during thermogravimetric analysis would be about 10%. Furthermore, published data indicate that the TG curves for dehydrating goethite or lepidocrocite differ from those observed in our experiments.[11,12] Typically, when heated to 200°C, there is an initial mass loss of no more than 5% due to the loss of adsorbed water, followed by a sharp inflection in the TG curve and a total mass loss of about 10%. Moreover, dehydration, in contrast to the iron(III) hydroxide precipitates obtained in this work, occurs in a single step.[11,12] Taking into account the above, we can conclude that in our experiments, iron(III) hydroxide was formed with the general (gross) formula $Fe_2O_3 \times 2H_2O$ with a minor admixture of goethite, lepidocrocite, and magnetite.

The formation of iron(III) hydroxide with the general (gross) formula $Fe_2O_3 \times 2H_2O$ was previously found in the works.[13,14] At the same time, the precipitate obtained in[14] was X-ray amorphous. The absence of OH groups in iron(III) hydroxide precipitates obtained from ammonia solutions at pH 10 and 13 was established by IR spectroscopy in the work.[13]

Thus, since the resulting iron(III) hydroxide precipitates ($Fe_2O_3 \times 2H_2O$) are amorphous and cannot be detected by X-ray diffraction analysis, the diffraction patterns (Fig. 2) only contain lines characteristic of goethite (α-FeOOH) and lepidocrocite (γ-FeOOH), which are present in the precipitates in small quantities and are probably impurities. Consequently, calculations of the phase composition of the precipitates based on X-ray diffraction data are incorrect. The low content of goethite (α-FeOOH) and lepidocrocite (γ-FeOOH) in the precipitates apparently explains the absence of bands characteristic of these compounds in the Raman spectra. The modes observed at 3740 cm^{-1} in Fig. 4 can be attributed to goethite

(α-FeOOH) and lepidocrocite (γ-FeOOH). The low intensity of these modes also confirms that these phases are present in the precipitates in small quantities.

Fig. 6 shows the effect of pH on the zeta potential of iron(III) hydroxide precipitate particles formed in the solution. It is evident that the zeta potential of the iron(III) hydroxide precipitate particles formed in our experiments at pH<5.4 has a positive value, and at pH>5.4 it becomes negative (curve 1). The point of zero charge corresponds to pH 5.4. This finding aligns with data[7] for iron(III) hydroxide in the form of two-line ferrihydrite but significantly differs from results reported in previous studies,[15,16] where the pH of the zero charge point for ferrihydrite particles was found to be 8.4[15] and 8.8[16]. We attribute this discrepancy, as noted previously,[7] to the presence of sulfate ions in the model solution.

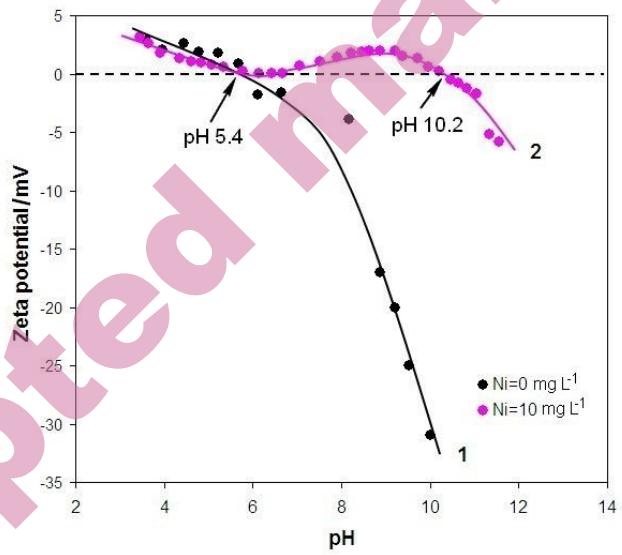

Fig. 6. Dependences of zeta potential of iron(III) hydroxide particles on the pH of the solution and concentration of nickel ions in it.

Fig. 6 also shows that at pH<5.4, the introduction of nickel ions into the solution has an insignificant effect on the zeta potential of iron(III) hydroxide particles (please see curves 1 and 2). This may indicate a weak adsorption of nickel ions on the surface of precipitate particles in this pH range. In contrast, at pH>5.4, the adsorption of nickel ions on the surface of iron(III) hydroxide precipitate particles increases, as indicated by the rise in zeta potential (curve 2). At pH>10, the adsorption of hydroxide ions begins to predominate, and the zeta potential of precipitate particles decreases (curve 2). This results in a shift of the point of zero charge to the alkaline region, reaching a value of 10.2.

It is noteworthy that a similar relationship was previously discovered in the work.[7] The study found an increase in the zeta potential of iron(III) hydroxide precipitate particles in the form of two-line ferrihydrite upon the introduction of nickel ions, accompanied by a corresponding shift in the pH of the zero charge point to the alkaline region.[7] Moreover, the pH shift of the zero charge point of iron(III) hydroxide particles when arsenic anions were introduced into the solution was also found in the work.[17] At the same time, due to the negative charge of arsenic anions, the zeta potential of the precipitate particles decreased, and the pH of the zero charge point shifted, respectively, to the acidic region.[17]

CONCLUSION

The studies of iron(III) hydroxide precipitates obtained at pH 7 and 8 from a solution of iron(II) sulfate in the presence of sodium sulfate (400 mg L^{-1}) indicate that they have the general (gross) formula $Fe_2O_3 \times 2H_2O$, along with the presence of small amounts of goethite (α-FeOOH) and lepidocrocite (γ-FeOOH). This is supported by data from X-ray and thermogravimetric analyses, as well as Raman and IR spectroscopy.

The zeta potential of the precipitate particles shows a positive value at pH<5.4, transitioning to a negative value at pH>5.4, indicating that the point of zero charge occurs at pH 5.4. Notably, the introduction of nickel ions into the solution results in a second point of zero charge at pH 10.2.

Furthermore, the sorption of nickel ions onto the iron(III) hydroxide precipitates does not involve chemisorption. Thus, no mixed compounds between iron and nickel are formed during the precipitation.

Acknowledgements: This work was carried out in accordance with the assignment by the Ministry of Science and Higher Education of the Russian Federation (theme No. 124020600024-5) and also supported by Government of the Sverdlovsk region and the grant of Russian Fund for Basic Research (Project No. 20-48-660038).

И З В О Д

УКЛАЊАЊЕ НИКЛ(II) ЈОНА ТОКОМ ПРЕЧИШЋАВАЊА ВОДЕ ГВОЖЂЕ(II) СУЛФАТОМ. 2. ДЕО. СТРУКТУРА И САСТАВ ПРЕЦИПИТАТА ГВОЖЂЕ(III) ХИДРОКСИДА

OLEG D. LINNIKOV, IRINA V. RODINA, GALINA S. ZAKHAROVA, INNA V. BAKLANOVA, YULIA V. KUZNETSOVA, ALEXANDER P. TYUTYUNNIK, ZILARA A. FATTAKHOVA

Institute of Solid State Chemistry, Ural Branch of the Russian Academy of Sciences, Pervomayskaya St., 91, 620990, Ekaterinburg, Russia.

Спроведена је упоредна анализа састава и структуре свеже исталожених преципитата гвожђе(III) хидроксида добијених из раствора гвожђе(II) сулфата у присуству натријум-сулфата (400 mg L^{-1}) на pH 7 и 8, пре и после сорпције јона никла. Коришћењем ИЦ и раманске спектроскопије, фазне рендгенске и термогравиметријске анализе показано је да талози имају општу (бруто) формулу $Fe_2O_3 \times 2H_2O$ и садрже малу количину гетита (α-FeOOH) и лепидокрокита (γ-FeOOH). Утврђено је да сорпција јона никла на овим талозима

није праћена хемисорпцијом, тј. не долази до формирања мешовитих једињења гвожђа и никла. Тачка нултог наелектрисања честица талога налази се на pH 5,4, при чему је зета потенцијал позитиван испод, а негативан изнад ове вредности pH. Увођење јона никла у раствор доводи до појаве друге тачке нултог наелектрисања на pH 10,2.

(Примљено 7. априла; ревидирано 28. априла; прихваћено 30. октобра 2025.)

REFERENCES

1. O. D. Linnikov and I. V. Rodina, *J. Serb. Chem. Soc.* (2025) (https://doi.org/10.2298/JSC250407080L)
2. M. Kiyama, T. Takada, *Bull. Chem. Soc. Japan* **45** (1972) 1923-1924
3. T. Misawa, K. Yashimoto, S. Shimodaira, *Corrosion Science* **14** (1974) 131-149
4. Y. Deng, *Water Res.* **31**(6) (1997) 1347-1354 (https://doi.org/10.1016/s0043-1354(96)00388-0)
5. R. R. Kleshcheva, D. A. Zherebtsov, V. Sh. Mirasov, D. G. Kleshchev, *Bull. South Ural State Univ.* **1** (2012) 17-22. [in Russian].
6. E. V. Petrova, A. F. Dresvyannikov, M. A. Tsyganova, A. M. Gubaidullina, D. V. Wasserman, N. I. Naumkina, *Bull. Kazan Techn. Univ.* **2** (2009) 24-32. [in Russian].
7. O. D. Linnikov, I. V. Rodina, G. S. Zakharova, K. N. Mikhalev, I. V. Baklanova, Yu. V. Kuznetsova, A. Yu. Germov, B. Yu. Goloborodskii, A. P. Tyutyunnik, Z. A. Fattakhova, *Water Env. Res.* **94**(12) (2022) e10827 (https://doi.org/10.1002/wer.10827)
8. M. Hanesch, *Geophys. J. Int.* **177** (2009) 941-948 (https://doi.org/10.1111/j.1365-246X.2009.04122.x)
9. D. L. de Faria, S. S. Venâncio, M. T. de Oliveira, *J. Raman Spect.* **28** (1997) 873-878 (https://doi.org/10.1002/(SICI)1097-4555(199711)28:11<873::AID-JRS177>3.0.CO;2-B)
10. M. A. Legodi, D. de Waal, *Dyes and Pigments* **74** (2007) 161-168 (https://doi.org/10.1016/j.dyepig.2006.01.038)
11. M. Kosmulski, S. Durand-Vidal, E. Mazcka, J. B. Rosenholm, *J, Col. Interf. Sci.* **271** (2004) 261-269 (https://doi.org/10.1016/j.jcis.2003.10.032)
12. E. Paterson, R. Swaffield, *J. Therm. Anal.* **18**(1) (1980) 161–167 (https://doi.org/10.1007/bf01909464)
13. M. V. Akhmanova, G. I. Malofeeva, N. P. Andreeva, *J. Anal. Chem.* **31**(3) (1976) 447-453 [in Russian].
14. L. G. Berg, K. P. Pribylov, V. P. Egunov, R. A. Abdurakhmanov, *Russian J. Inorg. Chem.* **14**(9) (1969) 2303-2306 [in Russian].
15. J. Liu, R. Zhu, L. Ma, H. Fu, X. Lin, S. C. Parker, M. Molinari, *Geoderma* **383** (2021), 114799 (https://doi.org/10.1016/j.geoderma.2020.114799)
16. M. Villalobos, J. Antelo, *Revista Internacional de Contaminacion Ambiental* **27**(2) (2011) 139-151 (https://doi.org/10.20937/RICA.25013)
17. M. A. Inam, R. Khan, K-H. Lee, Y-M. Wie, *Int. J. Env. Res. Pub. Health* **18** (2021) 9812 (https://doi.org/10.3390/ijerph18189812).